Properties and combustion characteristics of bio-oils from catalytic co-pyrolysis of grape seeds, polystyrene and waste tires.

Álvaro Muelas[1], Diego Aranda[1], María Soledad Callén[2], Ramón Murillo[2], Alberto Veses[2], Mohamad Asrardel[1], Javier Ballester[3]*

[1] Laboratory of Research on Fluid Dynamics and Combustion Technologies (LIFTEC), CSIC – University of Zaragoza

[2] Instituto de Carboquímica (ICB-CSIC)

[3] Fluid Mechanics Group / LIFTEC, CSIC-University of Zaragoza

* CORRESPONDING AUTHOR:

Álvaro Muelas

Laboratory of Research on Fluid Dynamics and Combustion Technologies (LIFTEC)

María de Luna, 10, 50018-Zaragoza - Spain

Phone: 976506520 (Ext: 247)

amuelas@liftec.unizar-csic.es

KEYWORDS: co-pyrolysis, biomass, waste tires, polystyrene, Calcium based catalyst, droplet combustion, soot

ABSTRACT

This work aims to study the bio-oils obtained from the catalytic co-pyrolysis of waste polymers and a residual biomass (Grape Seeds, GS). For that purpose, the organic liquid fractions produced in an auger reactor were thoroughly characterized in two steps, obtaining in the first place their main physicochemical properties as well as their chemical compositions and secondly their droplet combustion behaviors. Both the polymer type (Waste Tires or Polystyrene, WT and PS respectively) and the nature of the low-cost, Calcium-based catalyst used (Carmeuse limestone, calcined dolomite or an inert material such as sand) were studied. A significant improvement in the physicochemical properties of the bio-oils was obtained when using a catalyst, with lower viscosity, density and oxygen content. These beneficial effects were more marked for the bio-oil produced with the Carmeuse catalyst, presumably due to the higher prevalence of aromatization and hydrodeoxygenation reactions. When changing the polymer source from WT to PS, a considerable increase in the aromatic content and a viscosity reduction was noted. The droplet combustion tests revealed the consistent occurrence of microexplosions for all the studied bio-liquids, being these bursting events more violent for the GS-PS oil. Regarding the evaporation behavior, this liquid also yielded significantly higher burning rates during the initial heat-up phase, in agreement with its richer composition in volatile compounds such as styrene. These results point to this fuel as the one with the best global combustion behavior from all the explored bio-oils. The GS-WT liquids showed much closer features among them, although with noticeable differences depending on the catalyst used. A more volatile behavior was observed for GS-WT Carmeuse, followed by GS-WT Dolomite and GS-WT Sand, strengthening thus the previously reported improvements in physicochemical properties. Finally, the propensity to form soot of these bio-oils was characterized through a soot probe, which revealed a higher soot yield for the bio-liquids produced with the Carmeuse catalyst.

1. INTRODUCTION

The use of biomass as a feedstock in a pyrolysis process is a well-known and promising technology to reduce the current dependence on fossil fuels, while also being a renewable and carbon-neutral energy source [1, 2]. The pyrolysis of biomass yields biochar, gases and vapors [3] that after cooling can be condensed into a liquid product known as bio-oil or, alternatively, pyrolysis liquid or pyrolysis oil.. Bio-oil has been extensively studied in the literature, either as a standalone fuel or as a mixture, in diverse applications such as boilers, furnaces, diesel engines or even turbines (e.g., see [4, 5, 6]). Studies regarding computational simulation of waste and biomass pyrolysis have also been carried out in different types of reactors [7-9]. However, some bio-oil properties imply important drawbacks, which severely hinder their use in many combustion applications [2, 3, 10, 11]: high acidity and corrosivity, low heating value, high water content, immiscibility with conventional fuels and high viscosity. Moreover, bio-oils typically display a significant content of solid particles and a bad storage behavior due to aging. Most of these undesirable properties arise from the high oxygen content of the fuel, which generally ranges between 35-60% wt. [2]. It would be most desirable, therefore, to remove the oxygenated compounds, upgrading the bio-oil properties. Different upgrading strategies, such as hydrodeoxygenation, fast catalytic pyrolysis, hydrogenation, catalytic cracking and molecular distillation are considered to be promising technologies which can overcome these challenges [12, 13].

An alternative strategy to obtain an upgraded bio-oil is the co-pyrolysis of biomass with other carbon-rich wastes, such as waste tires or plastics, allowing for the production of a stable oil [14]. Recent reviews such as [2, 15] provide valuable information on this technology, which can produce a better quality fuel when compared with traditional fast pyrolysis of neat biomass, primarily because of the much lower oxygen content and higher heating value of these co-pyrolysis liquids [13, 16]. A further advantage of this approach is

that the polymer wastes used as a feedstock in the pyrolysis plant are valorized through this process. This is especially beneficial for the case of using waste tires, as they pose a major environmental problem due to the huge number of end-of-life tires produced every year (in the range of 1 billion units worldwide [17]), the technical difficulties involved in their recovery and recycling [18] and the high risks associated with their disposal in landfills (which, in fact, is banned in the EU in accordance with the Council Directive 1999/31/EC).

In spite of these advantages, the bio-oils obtained through co-pyrolysis of biomass and waste polymers still require further upgrading in order to be considered as drop-in fuels for most combustion applications [13, 19]. A significant improvement of the oil properties can be obtained when using a suitable catalyst within the co-pyrolysis process. This strategy appears to be a promising option for upgrading the bio-liquids while keeping the production process in a single step, as it is detailed in recent reviews such as [19, 20]. In fact, the use of low-cost Calcium-based catalysts has been studied by this group for the catalytic co-pyrolysis of grape seeds and two different waste polymers (waste tires and polystyrene) in previous works, both in a lab-scale reactor [21, 22] and in a Technology Readiness Level 5 (TRL-5) auger reactor [13, 23]. The encouraging results obtained in these studies support this technology for obtaining high-quality bio-oils with a heating value comparable to that of conventional fossil fuels and a very low oxygen content, suitable thus for direct use in certain combustion applications.

Since the main final use of these bio-oils is their energetic valorization, an assessment of their combustion characteristics is thought to be a valuable addendum to the more standard physicochemical analysis. For that purpose, the isolated droplet configuration has proven to be a useful benchmark for gaining knowledge on the combustion behavior of liquid fuels. The simplicity of this setup, with a single, isolated liquid droplet burning under fixed and well characterized conditions allows for a precise knowledge of all the relevant parameters

which affect the process. In comparison with the much more complex configurations occurring in real applications such as engines or boilers, this simplicity greatly facilitates the analysis of the underlying physics in fundamental studies, as well as allows for a precise characterization of the combustion behavior for different fuels in more applied works. This approach has been used in the literature for evaluating the combustion characteristics of many conventional and alternative fuels, such as diesel and biodiesel [24, 25], kerosene and aviation bio-fuels [26] or gasoline and butanol [27], among many others. For the case of bio-oils, it can be said that most of the effort has been directed to study the droplet combustion characteristics of liquids produced through conventional pyrolysis of lignocellulosic biomass. Extensive studies by Shaddix et al. [28, 29] explored the droplet combustion behaviors of a wide variety of flash pyrolysis liquids obtained from different feedstock (pine, oak, poplar, etc.). They obtained consistent microexplosions (i.e., a burst of the liquid droplet due to internal vaporization), which effectively shortened the droplet lifespan. However, the burning rates were significantly lower than those of a fuel oil No. 2, as it would be expected in light of the bio-oil properties displayed in [28]. It is noteworthy that these studies were performed in a drop-tube facility, where the 350 μm droplets were heated and ignited in free fall, without the influence of a suspending fiber which could promote heterogeneous nucleation of the vapors inside the droplet. A similar setup, although with considerably smaller droplets (in the range of 60 μm) was used by Garcia-Perez et al. [30] for evaluating the combustion characteristics of biomass vacuum pyrolysis liquids. Similarly to [28, 29], the bio-oils burning rates were noticeably lower than those of a fuel oil No. 2, but in this case the authors did not observe complete microexplosions, reportedly because of the lower heating rates and smaller droplet sizes. Interestingly, Garcia-Perez et al. [30] studied the formation of residual carbonaceous solids, with sizes which could even surpass that of the initial droplet diameter. On the other hand, Shaddix et al. highlighted in [28] the important role of the reported

microexplosions in reducing or even eliminating the production of coke cenospheres, which can be highly problematic for many combustion applications. Other single droplet works such as [31-33] relied on the suspended droplet technique, with puffing and bubbling phenomena rather than the proper microexplosions reported in [28, 29]. It is important to note, therefore, that the experimental conditions used in the droplet combustion tests can significantly modify the observed behaviors.

As pointed out, bio-oils produced through conventional pyrolysis show wide differences in chemical composition and properties when compared with liquids obtained by means of more novel technologies. A previous work [34] highlighted these differences for a tire pyrolysis liquid (TPL), which was found to display a much quicker conversion than the aforementioned bio-oils, with microexplosions and burning rates comparable to those extracted for a Spanish heating oil (i.e., fuel oil No. 2). To the best of the author's knowledge, this kind of droplet combustion characterization has not been performed for co-pyrolysis liquids of biomass and waste polymers. In light of the promising results of this technology to yield high quality and upgraded bio-oils, this study aims to evaluate the main combustion characteristics of different liquid fractions yielded from the catalytic co-pyrolysis of grape seeds and two kind of waste polymers (residual tires and polystyrene). In doing so, this work intends to provide data regarding the single droplet combustion behavior of these novel fuels under experimental conditions close to those occurring in real flames. Additionally, the effect of the catalyst used in the co-pyrolysis process will be also assessed, namely by comparing the droplet combustion behaviors of three bio-oils obtained under exactly the same experimental conditions, with the only change of the catalyst. Two different Calcium-based catalysts will be tested for this purpose, in addition to a reference case where no catalyst was used in the co-pyrolysis. Besides the more common droplet combustion characteristics, such as the droplet and flame size evolution curves or the burning rates, the experimental results will also

report complementary behaviors which are thought to be of special relevance for this kind of fuels, such as the occurrence and typology of microexplosions, the potential formation of carbonaceous solid residues and a quantification of the soot yielded for each oil under high temperature and reducing conditions.

2. MATERIALS AND METHODS

2.1. BIOMASS, WASTE MATERIALS AND CATALYSTS

The biomass used was grape seeds GS (Vitis vinifera), a residue from the wine industry of the north-east area of Spain. Previous to its use, it was dried by reducing moisture content below 2 wt%. Regarding to the waste materials, two different materials were utilized. On the one hand, polystyrene PS (Acteco Productos y Servicios S.L.), which was obtained from food packaging and, on the other hand, rubber produced in the shredding of passenger car tires (WT), which was received in granulated form, without the steel thread and textile netting. It is worth to mention that the particle sizes of the three materials were similar, around 2−4 mm.

The main properties (proximate and ultimate analysis and heating value) of the different feedstocks are summarized in Table 1. The proximate analysis of the raw material was determined according to UNE-EN ISO 18134-3, UNE-EN ISO 18122 and UNE-EN ISO 18123 for moisture, the proportion of ashes and the volatile matter, respectively. The fixed carbon was calculated by difference. The ultimate analysis of the different materials was determined according to UNE EN 5104 in a Thermo Flash 1112 and the oxygen content was obtained by difference. The calorific value (LHV) was measured experimentally using an IKA-2000 calorimetric pump according to the Spanish standard procedure (UNE) UNE 164001 EX. As it can be observed in Table 1, remarkable differences among the three raw materials were observed. Whereas GS were characterized by a high oxygen content (37.2 wt%), involving a low LHV (20.5 MJ/kg), WT and PS showed a high carbon content and a

low oxygen content, implying heating values similar to or even higher than those obtained from fossil fuels.

In this study, two different Calcium-based catalysts (particle size distribution ranged between 300 μm and 600 μm) obtained from the calcination at 900 ºC of limestone (Carmeuse) and dolomite were selected based on their low cost, their environmental friendliness (CO_2 capture effect inherent to these catalysts) and their reusability nature. Both low cost catalysts were commercially available and were purchased through different private companies located in Spain. These catalysts have been previously described [13, 23] by the following techniques: X-ray diffraction (XRD), N_2-physisorption, mercury porosimetry [35, 36], Temperature Programmed Desorption of ammonia (NH3-TPD), Temperature Programmed Desorption of carbon dioxide (CO2-TPD) [37] and Inductively Coupled Plasma-Optical Emission Spectroscopy (ICP-OES). Detailed information about catalysts properties can be also found in the supplementary data (Tables S.1 and S.2).

Table 1. Main properties of grape seeds (GS), polystyrene (PS) and waste tires (WT).

	GS[1]	PS[1]	WT[1]
Moisture (wt%)	6.3	0.3	0.9
Ash (wt%)	4.3	0.9	7.0
Volatile matter (wt%)	65.1	98.4	63.0
Fixed Carbon (wt%)	24.3	0.4	29.3
Ultimate analysis (wt%)			
C	53.9	92.1	84.1
H	6.6	7.75	7.4
N	2.2	0.12	0.5
S	0.1	0.0	1.7
O	37.2	0.03[2]	3.4
HHV (MJ/Kg)	22.1	41.1	37.3
LHV (MJ/Kg)	20.5	39.4	35.7

[1]: As received (Air-dried basis); [2]: Calculated from ultimate analysis by difference

In this research, two different variables that affect the catalytic co-pyrolysis of biomass and waste polymers were studied. First, the influence of the polymer type was assessed

performing co-pyrolysis experiments with GS-WT and GS-PS (80:20 mass ratio for the two feed mixtures). Process conditions were identical for both feedstocks and the same catalyst was used (Carmeuse). In addition, the influence of catalyst nature was also studied performing three tests with the same feed mixture (GS-WT mixture, 80:20 mass ratio) and using the two low cost catalysts (Carmeuse and dolomite) (fuel to catalyst ratio, 2:1 mass basis) as well as sand (particle size distribution between 2-6 mm), which acted as a blank reference in order to ascertain the effect of not using any catalyst.

2.2 PILOT PLANT

All experiments were performed in a pyrolysis pilot plant (100 kW_{th}) consisting of an auger reactor working at atmospheric pressure, using N_2 as carrier inert gas, with a feedstock feeding of 2 kg/h at 550ºC. The duration of each experiment was set at 2 h and the solid residence time was 7 min. To guarantee the repeatability of the tests, two runs were performed, ensuring a RSD < 5%. Extended information about the pilot plant can be found elsewhere [13]. Briefly, two independent stirred hoppers provided with screw feeders regulate the mass flow of the different feedstocks. One of them is used to feed the mixture composed of GS and waste polymer and the other one feeds the low cost catalyst. Prior to the experiments, the feeding was carefully mixed and then was added to the hopper, ensuring a good homogeneity. Based on the maximum deoxygenation rate reached in the organic fraction, a feedstock to catalysts ratio of 2 was fixed for catalytic tests. Particularly, the catalysts were diluted with sand, keeping a (sand + catalyst) to feedstock ratio of 3:1. This stock of solids has been calculated as the minimum amount of heat carrier required for a self-sustainable process from an energy perspective [38, 39]. Three independent electrical resistances surrounding the reactor provide the energy needed for the pyrolysis process. In addition, a control and acquisition system allowed monitoring 4 pressure transducers and 10 thermocouples located in strategic points of the pilot plant. While the remaining solid after

pyrolysis is collected in a closed hopper, the released gas leaves the reactor and is conducted to a condenser where the pyrolytic oil is collected. The non-condensable gas is cleaned and conducted to a flare. All conversion products but gas are weighed and stored in closed containers or bottles under inert conditions for further use and analysis.

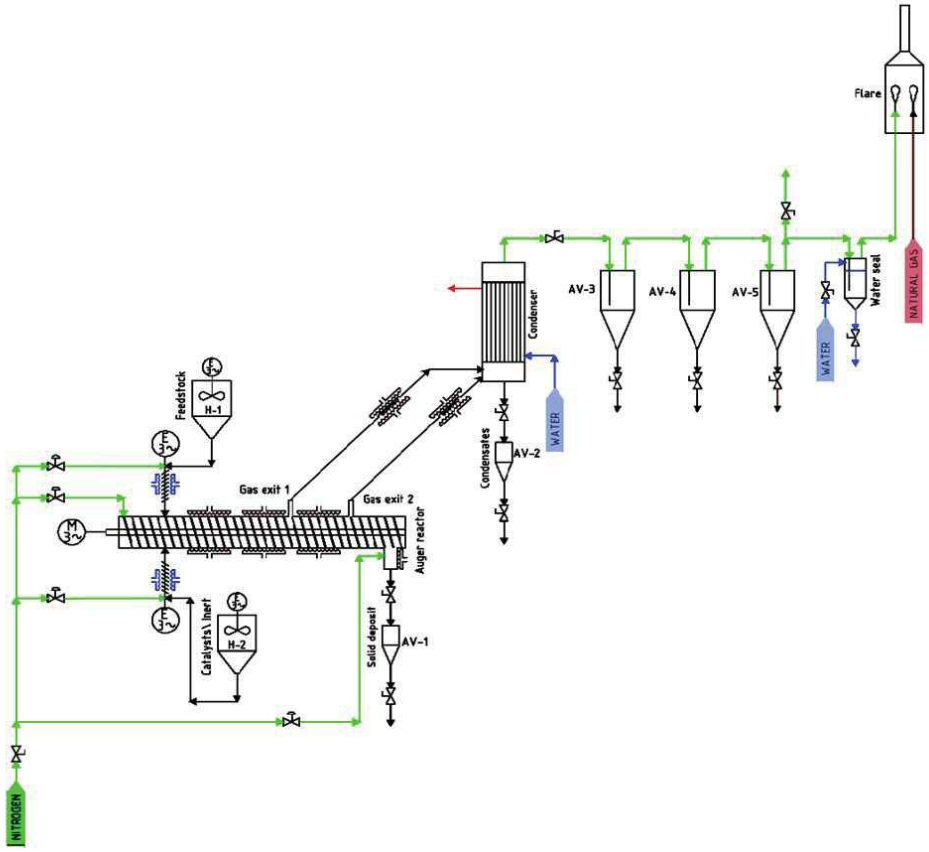

Figure 1. Process flow drawing of the pilot plant used for catalytic co-pyrolysis experiments.

2.3 PRODUCT CHARACTERIZATION

The three conversion products (liquid, solid and gas) obtained after the co-pyrolysis experiments were characterized. Because details regarding to the gas and solid fraction have been previously reported [13, 23], this research was mainly focused on the liquid fraction analysis and use. Hence, the liquid fraction was a heterogeneous sample composed of two differentiable phases: organic and aqueous. These phases were separated after centrifugation at 2000 rpm for 10 min and further decantation (organic

phase at the top and aqueous phase at the bottom). The organic phase was analyzed, according to standard methods, to determine different physicochemical properties. The ultimate composition (Carlo Erba EA1108), calorific value (IKA C-2000), water content by Karl-Fischer titration (Crison Titromatic) according to ASTM E203-96, pH (Mettler Toledo T50) and density (gravimetric method) were determined in triplicate.

The chemical composition of the organic phase was obtained by using gas chromatography coupled to mass spectrometry (Varian CP-3800 gas chromatograph and a Saturn 2200 ion trap mass spectrometer). A CP-Sil 8 CB low-bleed capillary column composed of 5% phenyl and 95% dimethylpolysiloxane was used (60 m, i.d. 0.25 mm, film thickness 0.25 μm). The injected samples were subjected to the following temperature/time program: 40 ºC for 4 minutes, a heating rate of 4 ºC/min until reaching a final temperature of 300 ºC for 21 minutes. BIP quality Helium was used as carrier gas at a constant column flow of 1 Nml/min and the respective temperatures for the injector, source and transfer line were 280 ºC, 200 ºC and 300 ºC. In all cases, 1 μl of sample was injected where 1:25 wt % was mixed with CH_2Cl_2:C_2H_6O (1:1 vol). A split ratio 25:1 and a solvent delay of 6.4 minutes were applied. Electron ionization mode at 70 eV and a range of 35-550 m/z was operated by the MS. Individual peaks were identified with the 2011 NIST library and each peak was quantified according to the corresponding m/z by normalization area (area of each peak versus the total area), to finally group compounds by different families. Samples were injected by duplicate and relative standard deviations for the different families varied between 0.15-17%.

2.4 DROPLET COMBUSTION FACILITY

After production and characterization of the different co-pyrolysis liquid fractions, their most relevant evaporation and combustion features were explored by means of

single droplet combustion tests. These tests were performed on a drop tube rig developed at LIFTEC, and described in detail in a previous work [40]. A scheme depicting the main elements of the setup is presented in Figure 2.

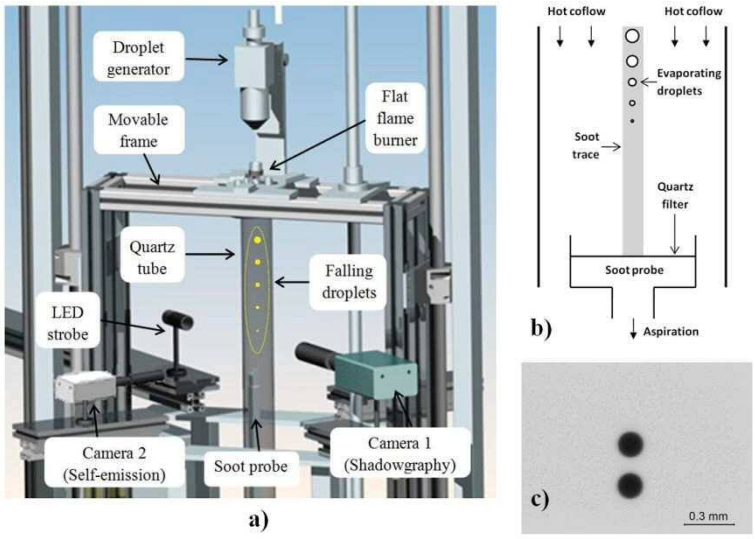

Figure 2. Droplet combustion facility (DCF) scheme, displaying its main components (a); Diagram depicting the soot probe operation (b); Double-exposure photograph of a free-falling GS-PS oil droplet (c).

A stream of free-falling droplets was generated in a piezoelectric device, which achieved initial nominal diameters (d_0) of 150 μm and a separation between consecutive droplets always greater than 100 diameters. This separation, in combination with the low relative velocity droplet-coflow, ensured that each droplet remained unaffected by the others during its whole lifespan. The hot coflow was provided by a McKenna premixed flat-flame burner, being the free-falling droplets directly introduced within its combustion products by means of an injection orifice passing through the sintered burner plug. Once surrounded by this hot coflow, the droplets evaporated and burned along a cylindrical quartz combustion chamber axis. The burner was fed with methane and air in

different proportions depending on the oxygen availability desired in the coflow. As this work intends to study the evaporation and combustion behavior of the different oils under conditions as representative as possible of those occurring in final applications such as boilers, a realistic environment was sought in terms of both gas temperature and composition. Thus, three different oxygen levels were used for this study, namely a pure evaporation condition (i.e., 0% O_2), and two combustion cases, with 3 and 5% O_2 (vol., dry basis) in the coflow. The first condition was obtained through the burning of a stoichiometric mixture of methane and air at the flat-flame burner, whereas for the latter cases a slight air excess was employed to yield unburned O_2 in the flue gas. The temperature profiles for these three conditions can be found in Appendix C of the Supplementary materials of [40], where it can be observed that most of the droplet evolution occurs under gas temperatures of the order of 1600-1700 K.

The droplet evaporation and burning processes were recorded by means of three different optical setups, each of them aiming to capture different features. A backlit CCD camera (QImaging Retiga SRV, Camera 1 in Figure 2a) fitted with a telemicroscope was used to obtain the droplet size and velocity by working through the double-exposure technique, as displayed in Figure 2c. This kind of pictures were processed in Matlab to extract the data in an accurate and repeatable way. Additionally, a CMOS camera (Hamamatsu C11440-36U, Camera 2 in Figure 2a) recorded the diffusion flame formed around each droplet, as it will be shown in Section 3.2. A third optical setup captured the macroscopic flame traces created by the free-falling droplets, as it will also be displayed in Section 3.2. This rig consisted in a Teledyne DALSA Genie Nano C4060 fitted with a NIKKOR 18-105mm f/3.5-5.6G ED lens.

Besides exploring the evaporation and burning behaviors of the different oil samples, their propensity to form soot was also characterized through a particle sampling probe.

This probe was developed and described in detail in [41], and therefore only its main features are summarized here. A scheme depicting its operation is presented in Figure 2b, where it can be observed that the probe collects all the soot particles which are formed along the droplets lifespan. In order to prevent soot oxidation, these tests were always performed at the 0% O_2 condition, and therefore the collected soot particles correspond to the pyrolysis of the fuel's vapors within an inert, hot coflow which allowed soot formation but inhibited its consumption. The soot agglomerates were retained on a quartz microfiber filter, which was subsequently dried at 110 °C for over 24 hours. The weighing of the dried filter with and without soot provided the soot mass collected during the test. Due to the small amount of soot weighed, special care was taken in order to prevent that room humidity could affect the results, as it was found that the quartz filter was hydrophilic. For that reason, the weighing procedure was performed inside a controlled-humidity room, with relative humidity levels always in the order of 15%. The analytical scale used was a Sartorius CP225D with a repeatability of ±20 μg. As introduced in [41], a soot index named *isolated droplet soot yield* (IDSY) and expressing the weight of soot produced per unit of injected fuel, was obtained for each oil, providing therefore a quantitative metric regarding their propensity to form soot.

3. RESULTS AND DISCUSSION

3.1. PROPERTIES AND CHEMICAL COMPOSITION OF THE ORGANIC FRACTION

Although the main aim of this research was focused on studying the combustion of the organic fractions, it was also interesting to relate them with the properties and the chemical composition based on two different effects. On the one hand, the influence of the catalyst on the co-pyrolysis GS-WT with an inert heat carrier like sand and with two different low cost catalysts: Carmeuse lime and dolomite. On the other hand, the influence of two different

waste materials, WT and PS, in the co-pyrolysis with GS, using the same catalyst: GS-WT Carmeuse and GS-PS Carmeuse. The main properties of the organic fraction for the different samples and catalysts are shown in Table 2.

Table 2. Properties of the organic fraction after the non-catalytic and catalytic co-pyrolysis processes.
LHV= lower heating value.

Experiment	Properties				Elemental Analysis (wt%)					
	H_2O (wt%)	pH	Viscosity (mPa.s)	Density (g/mL)	C	N	H	S	O	LHV (MJ/kg)
GS-WT (80:20) Sand	1.07±0.1	9.5	16.3±0.8	1.11	83.6±0.9	2.6±0.2	9.5±0.2	0.4±0.02	3.9±0.2	38.8±1.2
GS-WT (80:20) Carmeuse	0.62±0.1	9.1	3.5±0.2	0.91	87.0±0.8	2.5±0.1	9.6±0.2	0.4±0.02	0.5±0.1	40.7±1.5
GS-WT (80:20) Dolomite	0.76±0.1	9.1	5.6±0.3	0.98	84.9±0.4	2.8±0.2	10.0±0.1	0.6±0.03	1.8±0.2	40.1±1.4
GS-PS (80:20) Carmeuse	0.74±0.1	8.7	2.3±0.1	0.94	88.6±0.6	1.8±0.1	8.5±0.1	0.1±0.01	1.0±0.1	40.9±1.6

Table 2 shows how the water content of the organic fraction, depends on the catalyst type for the same co-pyrolysis mixture GS-WT. A decrease in the water content is observed with the Carmeuse catalyst compared to the non-catalytic process, whereas very similar results were obtained with the other catalyst, dolomite. This is directly related to the promotion of dehydration reactions by materials containing Calcium with poor total basicity and pure CaO crystalline phase without impurities [13]. According to the characterization techniques, the Carmeuse catalyst was a high purity material composed of CaO in a high percentage, 95 wt%, whereas dolomite was mainly formed by CaO (47.6 wt%) and MgO (33.2 wt%) [13]. In addition, a lower total basicity of the Carmeuse catalyst (0.04 mmol CO_2/g at 550ºC)

compared to the dolomite catalyst (0.11 mmol CO_2/g at 598ºC) would also justify the higher reduction in the water content. It was also observed that the addition of CaO in the co-pyrolysis of GS and WT rubber produced a remarkable decrease of the oxygen content (Table 2) compared to the non-catalytic process, sand. This fact corroborated the CaO dehydration capacity and the improvement of the organic phase by using this catalyst [13, 23]. Therefore, an increase of the heating value was reached, confirming that the co-pyrolysis of GS and WT rubber (80:20) with this Carmeuse catalyst provided better quality bio-oils.

When the same catalyst was compared for a different co-pyrolysis feedstock (GS-WT versus GS-PS), quite similar results were obtained for both. This could be justified by the similar nature of the materials, as WT is a copolymer of styrene, butadiene.

The influence of the catalyst on the viscosity (see Table 2) for the GS-WT experiments showed that both Calcium-based catalysts produced a remarkable decrease on this property compared to sand, this effect being most considerable for Carmeuse. When the influence of the waste material on the viscosity was compared, it was observed that lower viscosity was obtained for the co-pyrolysis of GS and PS than for the GS and WT mixture using the same catalyst, Carmeuse, indicating that this polymer, PS, improved the quality of the oil obtained versus the WT. As the bio-oil viscosity is widely dependent on the feedstock and pyrolysis conditions [42, 43], this improvement in the viscosity for the co-pyrolysis experiments could be explained based, on the one hand, on the feedstock (PS consists of volatile matter and almost no fixed carbon (Table 1) whereas that WT is made of styrene-butadiene copolymer, natural rubber and polybutadiene) and, on the other hand, on the nature and chemical composition of the bio-oils as shown in the next paragraphs.

According to the composition of the organic phase using GC-MS, a semi-quantitative identification of the compounds (relative area percentage) was carried out as it is shown in Table 3. A total of nine different families were identified for the co-pyrolysis of GS-WT

rubber without catalyst (sand) and independently of the catalyst used. These families were: aromatics, olefins, linear hydrocarbons HC, cyclic HC, phenols, esters, ketones, fatty acids and others. The aromatics constituted the group with higher percentage, being styrene, ethyl-benzene, toluene, xylene and benzene the main compounds [13].

The effect of the catalyst on the composition of the organic phase was reflected on the reduction of cyclic HC compared to the experiment with no catalyst (sand). In addition, an increase in the ketones family was observed. The Carmeuse catalyst increased the aromatic content compared to dolomite and to the non-catalyst experiment (sand), indicating that this type of catalyst promoted the aromatization and hydrodeoxygenation through ketonization and esterification reactions [13] producing a highly aromatic bio-oil and enhancing the potential use of the bio-oil as source of chemical products or as a drop-in fuel.

Table 3. The chemical composition of organic fraction analyzed by GC-MS in the co-pyrolysis and catalytic co-pyrolysis processes. HC: Hydrocarbons.

Experiment	Aromatics	Olefins	Linear HC	Cyclic HC	Phenols	Esters	Ketones	Fatty Acids	Others
GS-WT (80:20) (Sand)	64.5	2.7	0.4	23.6	5.0	0.8	0.1	1.0	1.8
GS-WT (80:20) (Carmeuse)	70.9	2.3	0.9	16.0	1.4	1.5	2.1	1.6	3.6
GS-WT (80:20) (Dolomite)	58.0	5.0	1.8	18.1	3.9	2.9	3.9	2.5	4.0
GS-PS (80:20) (Carmeuse)	96.9	-	0.2	-	0.3	0.4	0.8	0.2	1.2

When the comparison was based on the type of waste material used, WT and PS, it was observed that the GS-PS co-pyrolysis produced mainly aromatics [22], with a low

contribution of the other families (linear HC, phenols, esters, ketones, fatty acids and others). With regard to the aromatic compounds, styrene, ethylbenzene and toluene were the main compounds identified in the organic fraction (see Table S2, Supplementary information in [23]), all of them low-molecular weight aromatic compounds. As previously mentioned, these results could have a remarkable impact on the further use of this liquid, not only as a drop-in fuel but also as source of chemical products. The thermal scission of PS, linked to the promotion of H_2 transfer reactions, and the CaO effect, mainly attached to the dehydration and decarboxylation effects, seemed to justify the reduction of phenols and esters through hydro-deoxygenation route, being more remarkable in the case of GS-PS compared to the GS-WT Carmeuse experiment, obtaining a richer aromatic and more deoxygenated liquid. In addition, this effect was more remarkable in the case of GS-PS versus GS-WT due to the pure nature of the PS, whereas WT is composed of styrene butadiene co-polymer, natural rubber and polybutadiene. This composition for both, the GS-PS and the GS-WT bio-oils with Carmeuse catalyst, associated with more low-molecular weight components, could also explain the lowest viscosity obtained [44, 45] and the synergetic positive effects due to the presence of plastics and Calcium-based catalyst. At this point, it should be remarked the great improvement of bio-oil properties and chemical composition after the catalytic process. Thus, some of the main properties aforementioned were similar to those found for other commercial liquid fuels such as diesel [46].

3.2 DROPLET COMBUSTION RESULTS

This section aims to explore the single-droplet combustion behavior of each fuel by means of the Droplet Combustion Facility (DCF) described in Section 2.4. Besides the already presented four co-pyrolysis oils, this study will also include results for heating oil, which is considered a good representative of conventional fossil fuels used in many industrial and

residential applications. This fuel was thoroughly characterized in previous works, where its main isolated droplet characteristics were explored in detail [40] and even some surrogates were formulated in order to match them [41]. As the organic fractions obtained in this work are primarily intended for their burning in applications such as boilers, their comparison with heating oil seems appropriate, putting into perspective the behavior of these oils when compared with a well-characterized reference baseline. This fuel was the only one whose droplet evaporation experiment was repeated in order to check for the procedure repeatability. As detailed in [40], the comparison of both experimental runs yielded differences of 0.5% in droplet burnout times and 0.7% in time-averaged evaporation rates.

3.2.1 Droplet, flame and trace images

As it was described in Section 2.4, most information regarding the droplet combustion process is extracted from different optical setups. The first kind of pictures corresponds to the flame traces captured with a color camera operating with a long exposure time. Since all the studied fuels yield a significant amount of soot when exposed to the high temperature conditions applied at the DCF, these images display bright and orangish streaks caused by the black body radiation emitted from incandescent soot particles. The exposure time of these images is several times longer than the droplet generation period (40 ms), and therefore the integrated luminosity of multiple droplets is accumulated in the image, creating the flame traces which are presented in Figure 3 for all fuels at the 3% O_2 condition.

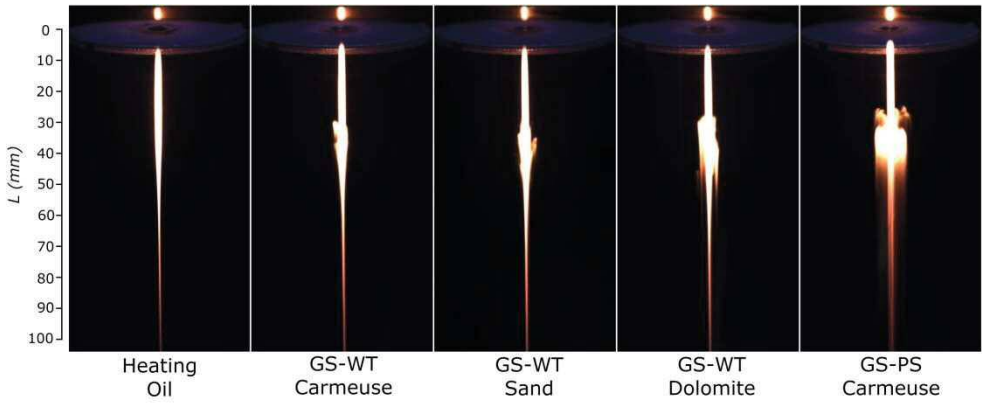

Figure 3. Long-exposure flame traces pictures captured for all fuels at the 3% O_2 coflow. The exposure time for all images is 200 ms (5 droplets injected during the exposure interval).

A first substantial difference can be noted in Figure 3 between heating oil and the rest of fuels. Whereas the former displays a smooth luminosity profile throughout all the combustion chamber, the four co-pyrolysis oils show abrupt microexplosions around 30 mm after the injection point. These microexplosions, which will be studied in detail later on in this same Section, completely shattered the droplets, causing a second atomization which can be noted in Figure 3 as an irregular broadening of the sooty luminous area. Among the four co-pyrolysis oils, GS-PS Carmeuse displayed the most violent microexplosions for all the oxygen conditions, with soot agglomerates being propelled further away from the combustion chamber's centreline. On the other hand, the three oils obtained from GS and WT yielded similar microexplosion intensities, although with slight differences regarding their occurrence point, as it will be detailed below. It is worth to note that these relative behaviors were maintained regardless of the O_2 condition explored.

The second kind of images are those captured with Camera 2 (Figure 2a), which aimed to record the individual envelope flames which surrounded the droplets. As it was discussed in a previous work [40], the black-body radiation emitted from soot particles is considerably more intense than the chemiluminescence emission from electronically excited radicals such as OH* or CH*, which are the most broadly accepted light-emitting species when it comes to

establish the flame position [47-49]. Given the high sooting tendency of the fuels studied here, soot emission heavily predominated in this kind of images, and therefore it would be more correct to speak of soot clouds rather than flame pictures. Soot particles are formed on the inner side of the shell flame, and therefore the light emission from excited radicals produced in chemical reactions would be located slightly further away from the droplet. In spite of this, and given the difficulty to capture this weak chemiluminescence emission for sooty fuels, several droplet combustion studies have indirectly estimated the flame position from the sooty emission (eg., [24, 25]). This will be also the case in this work, as its main objective is to obtain relative differences among the different bio-liquids, being the same kind of sooty flames captured (and measured) for all of them. A representative selection of these envelope flames is displayed in Figure 4 for all fuels under the 5% O_2 condition. The pictures are arranged in terms of their residence time normalized by the initial droplet diameter squared (t / d_0^2), as it is common practice in the droplet combustion literature in order to minimize differences arising from slight variations in d_0.

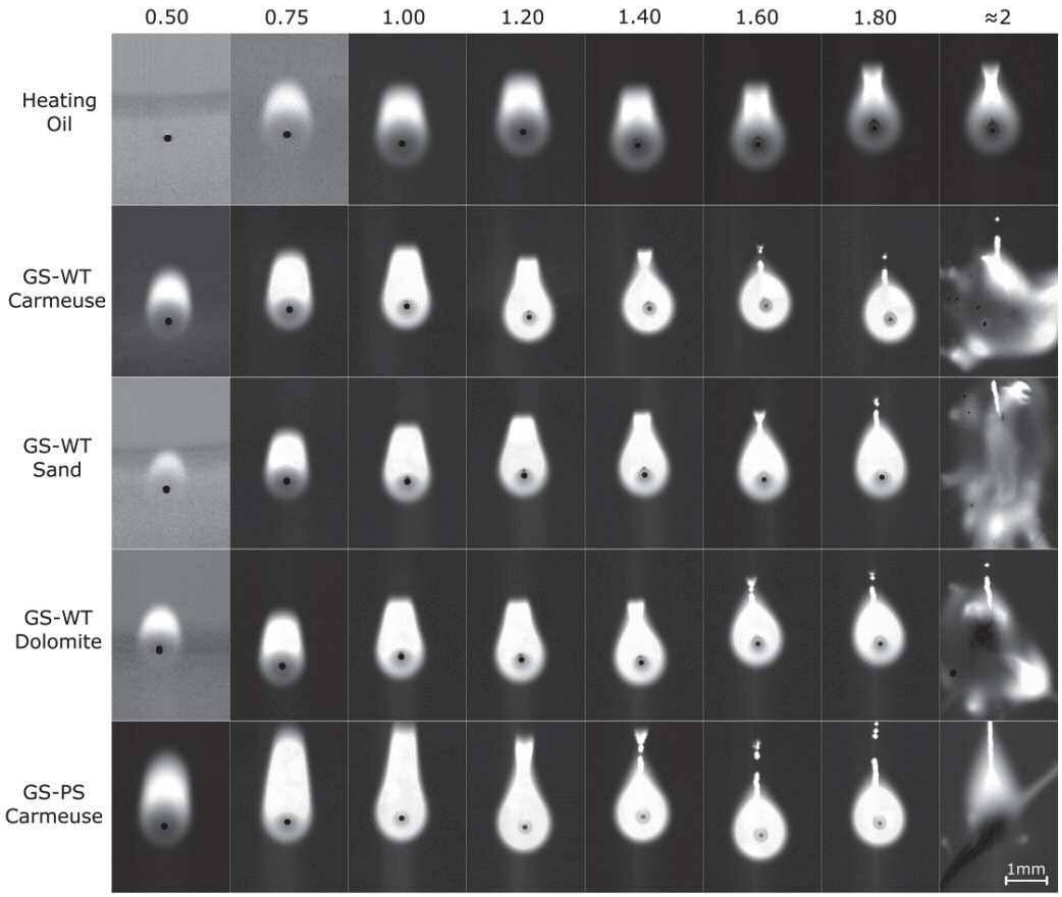

Figure 4. Individual droplets surrounded by their diffusion flames captured for all fuels at the 5% O_2 condition. Images are organized in accordance with their normalized time after injection*:* t / d_0^2 (s/mm^2).

Envelope flames in Figure 4 show distinct behaviors among fuels. The first and more obvious one is the occurrence of microexplosions for all the co-pyrolysis liquids around 2 s/mm^2 after injection, whereas heating oil displays a smooth evaporation until droplet depletion, as it was noticed in Figure 3. Regarding the onset of the flame, GS-PS Carmeuse displays a clearly more intense sooty emission already at 0.50 s/mm^2, followed by the GS-WT oils. No emission can be observed at that time for heating oil, whose ignition is in general delayed with respect to all pyrolysis oils. This points to a more volatile behavior of the GS-PS lighter fractions, which evaporate and ignite earlier than the rest of the fuels. Likewise, GS-WT Carmeuse would ignite slightly earlier than GS-WT Dolomite and GS-WT Sand, as inferred by the higher signal-to-noise ratio of its first picture (i.e., the flame appears

brighter and less noisy, whereas the background shifts to a darker tone after the contrast enhancement procedure). These observations concerning droplet ignition are consistent with the earlier onset of a flame trace in Figure 3.

Figure 4 also provides some qualitative information regarding the sooting propensity of each fuel. Even though quantitative data will be provided in the next Section, it seems interesting to analyze these features to prove if they are consistent with the subsequent soot probe measurements. For any given residence time, the GS-PS oil displays a more intense light emission. This envelope flame luminosity becomes brighter than that due to the backlight used with Camera 2, and therefore the liquid droplet becomes progressively eclipsed (as it can be observed by the clearer shade of the droplet). Additionally, GS-PS pictures display the longest soot trail for a given residence time, while also showing an earlier clustering of the soot trail's particles into thicker agglomerates. These soot agglomerates appear to exit the diffusion flame, forming an elongated soot tail which lags behind the free-falling droplet. The residence time when this clustering event happens is different for each fuel: GS-PS is the first one (1.40 s/mm^2), followed by GS-WT Carmeuse, GS-WT Dolomite and GS-WT Arena. Heating oil shows the onset of this soot clustering event only in its last picture (≈2 s/mm^2). Ranking the fuels according to this feature appears to provide very similar results as when sorting them in terms of sooty luminosity or even in soot trail length for a given residence time. This fact would suggest a higher soot yield for all the co-pyrolysis oils when compared with heating oil, pointing also to noticeable differences among them. These qualitative observations will be validated below with quantitative soot yield measurements.

The third kind of pictures obtained at the DCF are the backlighted, double-exposure droplet images captured with Camera 1 (Figure 2). The main aim of these pictures is to characterize the droplet size evolution, as it will be detailed in the next Section. However, through these

close-up images it is also possible to obtain valuable information regarding interesting phenomena such as microexplosion occurrence or the tendency to form soot particles. These two features can be observed in Figure 5, where a set of representative droplet images are presented according to their normalized residence time for all fuels at the 5% O_2 condition.

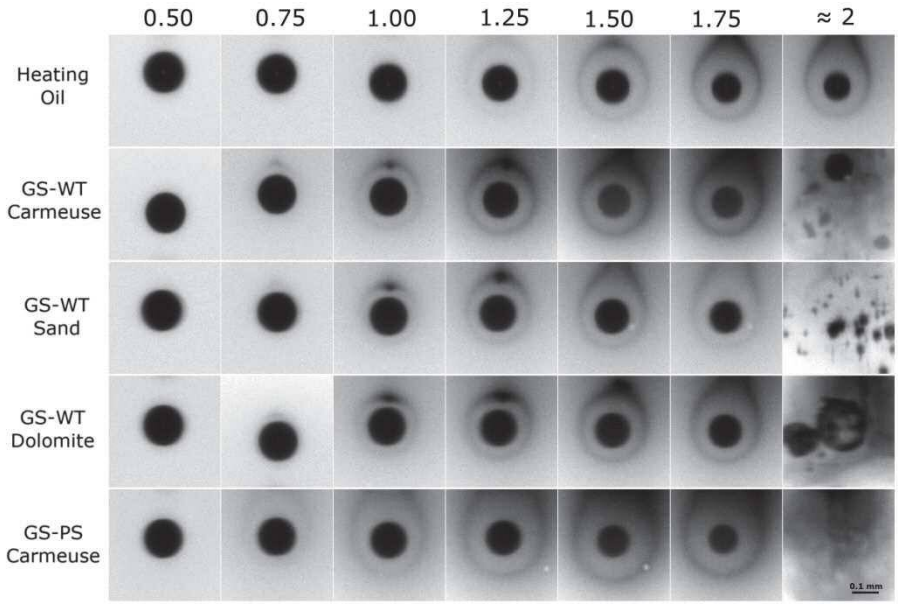

Figure 5. Individual droplets surrounded by soot shells for all fuels at the 5% O_2 condition. Images are cropped from the original double-exposure photographs, and organized in accordance with their normalized time after injection: t / d_0^2 (s/mm^2).

An interesting characteristic shared by all fuels in Figure 5 is the appearance of nearly spherical soot shells surrounding the droplets. As discussed in previous works (e.g., [34, 40]), the apparition of these soot shells is quite infrequent for droplet combustion tests at normal gravity, being generally a feature explored in experiments under microgravity conditions such as [24, 26-27]. However, the droplet sizes and small slip velocities applied in this work significantly reduced natural and forced convection effects, allowing for the formation of these structures (as detailed in [40]). The regions with a greater density of soot particles in Figure 5 reveal the places where the inwardly directed thermophoretic force is balanced by the outward viscous drag. As it can be noticed in Figure 5, the resulting soot shells are considerably spherical, pointing to a configuration close to spherical symmetry in the vicinity

of the droplet. Influence of natural or forced convection on the evaporation results presented in this work are thus expected to be negligible, which greatly facilitates comparison with 1-D droplet evaporation and combustion models (as assessed in Apendix A of the Supplementary materials of [40] for a set of tests performed under the same experimental conditions). It is also worth mentioning that these soot shells only occur under oxidizing atmospheres, being absent in the pure-evaporation case (the lack of an envelope flame lowers thermal gradients, causing much weaker thermophoretic forces). Likewise, the higher the O_2 availability in the coflow is, the stronger thermophoresis becomes, yielding thicker and more spherical soot shells (e.g., see [40]).

On the other hand it is also clear that, contrary to droplet combustion works under strictly controlled microgravity conditions, in the current study not all the soot particles are gathered at the radial equilibrium location, even for the 5% O_2 case depicted in Figure 5. The occurrence of a small slip velocity, in addition to buoyancy, tends to drag soot particles towards the trails analyzed in Figure 4. This fact has the advantage of clearing the camera view from an excessive amount of soot particles which could hinder droplet identification and measurement (as for example occurred in [26] for a kerosene). The analysis of the soot shells presented in Figure 5 should, however, take into account this soot leakage towards the droplet wake, complicating an assessment of the soot tendency based on the shell's thickness. If this leakage is assumed to be similar among fuels, the soot shells presented in Figure 5 would indicate a considerably lower soot production for heating oil in comparison with the co-pyrolysis liquids, as the soot shell onset is considerably delayed for this fuel.

Consistently with Figure 3 and Figure 4, another main difference noted in Figure 5 between the studied fuels is the occurrence of microexplosions for all the pyrolysis oils, whereas heating oil droplets evaporate smoothly until liquid depletion. This bursting feature will be

explored in detail through a collection of representative double-exposure images in Figure 6 for all the fuels which showed this phenomenon.

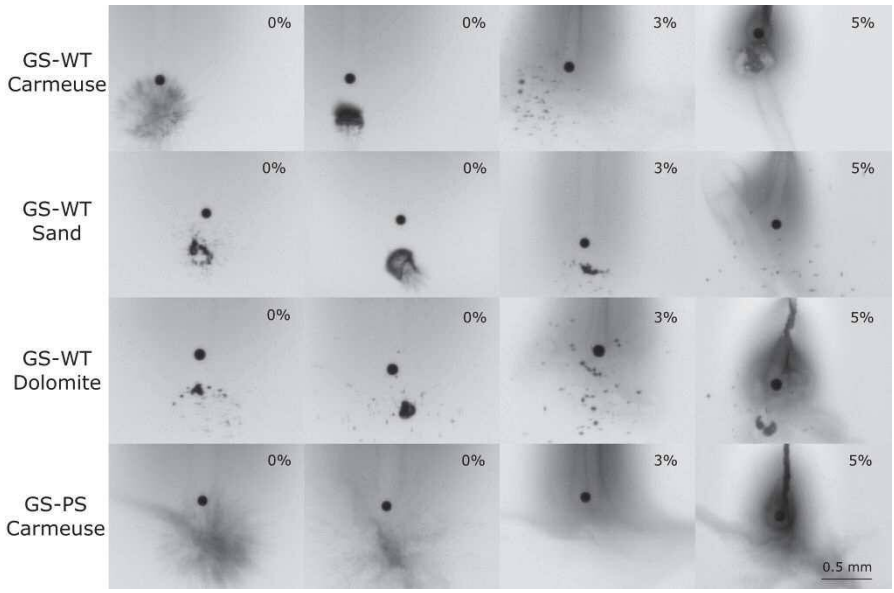

Figure 6. Double-exposure pictures of individual droplets microexploding for the bio- oils evaporating and burning under all oxygen conditions (O_2 level indicated for each image).

Each of the 16 double-exposure pictures arranged in Figure 6 was captured with a delay between shots of 500 μs, and therefore it can be considered that during that short time lapse the parent droplet evolves from a completely spherical shape to a collection of smaller droplets created through a second atomization process caused by the sudden internal vaporization of the lighter bio-oil fractions. To the best of the author's knowledge, this kind of result is novel for liquid fuels obtained through the co-pyrolysis of a biomass residue (GS) and waste polymers (WT and PS). When comparing the microexplosion images displayed in Figure 6 with those available in the literature for pyrolysis oils produced from biomass and waste tires, it seems clear that the droplet combustion experimental setup plays a relevant role. The sudden droplet breakups in Figure 6 show similarities with those reported at the same experimental facility for a tire pyrolysis liquid (TPL) in [34] or with the bio-oils tested

in [28] under a similar drop tube setup where unsupported, free-falling droplets were also exposed to a high temperature gaseous coflow. On the other hand, most of the experimental results available in the literature for bio-oils were obtained in setups where the droplet was attached to a solid filament. In this kind of studies (e.g., [31-33]), the microexplosion typology was reported to be quite different. Internal bubbling and puffing events swelled the droplet, but were not enough to trigger a second atomization into many child droplets, as it was noticed in the drop-tube tests. In this regard, the influence of the solid filament (which can act as a heterogeneous nucleation site) as well as the bigger droplets typically used in suspended droplet studies, are thought to be relevant regarding the occurring microexplosion typologies.

When comparing among the different co-pyrolysis oils in Figure 6, it seems clear that most of the reported microexplosions shattered the parent droplet, although with varying degrees of success. All the fuels were exposed to exactly the same experimental conditions, and therefore the different modes of microexplosions can be attributed to differences in the oil composition and properties. GS-PS displayed more intense microexplosions, being in most occasions the parent droplet atomized into a fine spray, without hint of any relevantly sized child droplet. This differential behavior is consistent with the more violent disruption event displayed in the flame traces of Figure 3.

The oils obtained from co-pyrolysis of GS and WT, on the other hand, displayed on average less violent secondary atomizations, being the liquid mass dispersed in a poorer manner for all of them compared to GS-PS. As a result, in Figure 6 it is possible to observe relatively big sub-droplets which could even be measured from these pictures. These kind of microexplosions for GS-WT oils are quite similar to those presented in [34] for a TPL. As it was reported in that previous work, no correlation was observed between the mode of microexplosion and the oxygen availability in the coflow (pictures presented in Figure 6

correspond indistinctly to 0, 3 and 5% O_2 conditions). Thus, the differences noted in Figure 6 for a given fuel appear to follow random patterns. This can be clearly noticed, for instance, for GS-WT Carmeuse, which shows an atomization spectrum ranging from a very efficient microexplosion (comparable to that described for GS-PS), to a situation more similar to a swelling and puffing event. These wide differences in the microexplosion mode for a given fuel at a fixed condition underscores the importance of stochastic aspects in this process, which become even more important for small-sized droplets such as those used in this study [50].

3.2.2 Quantitative data

As detailed in Section 2.4, the images recorded with cameras 1 and 2 (Figure 2) were processed in order to quantify the main combustion characteristics of the studied fuels in the most repeatable manner. The evolution of droplet size with time and the burning rate are presented in Figure 7 for the three oxygen conditions studied in this work (0, 3 and 5%). As introduced before, the first one corresponds to a pure evaporation case under oxygen-free and high temperature conditions, whereas the other two study the droplet combustion at oxygen levels which are representative of real combustion conditions in boilers (as it can be observed, e.g., in the oxygen maps experimentally measured in [51]). Results in Figure 7 are normalized by the initial droplet diameter (d_0), so that any small difference in d_0 between runs is minimized. Droplet size evolution curves are presented in the left column in terms of normalized square diameter versus normalized time, whereas the burning rates (K=-d(d^2)/dt) are displayed in the right column, also in terms of normalized time. The K values were calculated by fitting the d^2-t curves to a polynomial function which was subsequently derived with respect to time, yielding the temporal evolution of the burning rate. The fitting was performed through a least squares regression, with the polynomial order being chosen as the

minimum which allowed to correctly capture the data trend without introducing numerical artifacts unrelated to the problem physics (i.e., order 3 for the pyrolysis oils and 4 for heating oil).

As it can be observed in Figure 7, all the studied fuels show a steady decrease in droplet size until complete liquid depletion for heating oil, or until a sudden interruption occurs in the experimental curves for the pyrolysis liquids. This sudden interruption indicates the instant of droplet bursting, which consistently occurred for all the pyrolysis oils as described in Figure 6. Similarly to the reported data for a Tire Pyrolysis Liquid in [34], the instant of microexplosion was not completely fixed, but occurred randomly within an interval of the order of 0.1-0.2 s/mm^2. In that sense, the last experimental point for each run in Figure 7 corresponds to the last axial position where complete (and measurable) droplets were found.

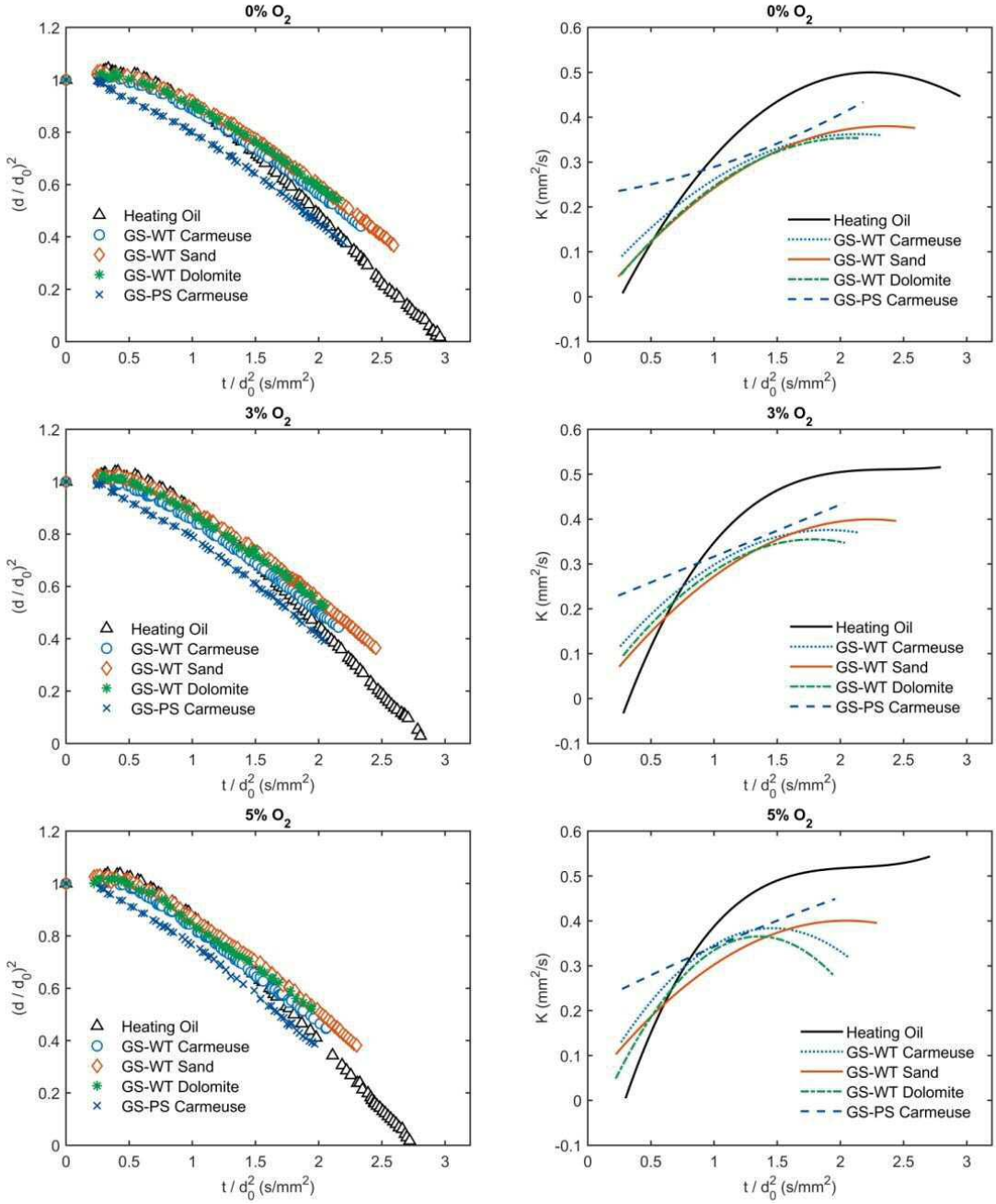

Figure 7. Normalized droplet size (left) and burning rate (right) evolution curves for all the fuels at the three studied oxygen conditions.

Heating oil, on the other hand, displays a more conventional evaporation behavior, with an initial droplet heating-up phase followed by a quasi-steady evaporation stage. During the first one, the liquid increases its temperature without practically any mass loss due to the low vapor pressure of heating oil when cold (the distillation curve of this fuel was experimentally measured in [41], with an initial distillation point of 233 °C). This droplet heating without

significant evaporation causes a slight increase in the droplet size during that first region, since the liquid density decreases with temperature. As the temperature increases, the onset of a strong evaporation starts to significantly reduce the droplet size, and the droplet progressively transitions towards the quasi-steady phase predicted by the well-known d^2-law. This transition can be better noticed in the *K*-*t* plot, where the burning rate of heating oil steadily increases until reaching a quite constant value.

The droplet evaporation behavior for the bio-oils reveals significant differences when compared with heating oil. In light of the heavy fragmentation incurred by the droplets at the bursting instant (Figure 6), it is expected that a total conversion of all the pyrolysis liquids occurs before that of heating oil. Even for low-efficiency microexplosions, where certain child droplets still display a relevant size, the strong dependency of evaporation time on droplet diameter (consumption times scale with the squared diameter) implies that total conversion is expected to occur close to the microexplosion instant. On the other hand, all the pyrolysis oils (and particularly GS-PS) appear to display higher evaporation rates during the initial heating-up stage, which does not show the thermal volumetric expansion noted for heating oil. This would mean a higher vapor pressure in cold conditions, as probably these liquids contain light fractions with relatively low boiling points. In spite of this faster evaporation onset, pyrolysis liquids increase their burning rates at a slower pace than heating oil, being their quasi-steady burning rate values also lower. However, as previously noted, the occurrence of a secondary atomization greatly enhances the liquid conversion through a sudden increase in the gas-liquid contact surface.

When comparing among the different pyrolysis liquids in Figure 7, GS-PS Carmeuse shows the most differential behavior, with a substantial higher evaporation during the initial stage (i.e, higher *K* values for short residence times). This would point to a richer composition in compounds with low boiling point when polystyrene is used as polymer

source in comparison with waste tires. However, the increase in K is slower than for GS-WS oils, being the burning rates relatively similar in the final stages prior to the microexplosion.

A comparison between the evaporation curves for GS-WS liquids reveals small differences among them, being the effect of the catalyst used in the co-pyrolysis process clearly less influential than the polymer feedstock. The GS-WT liquids also display quite similar evaporation behaviors to those reported in [34] for a tire pyrolysis oil. This result was not initially expected, as the liquids evaluated in the current work are obtained by a co-pyrolysis of only a 20% in mass of waste tires with 80% of grape seeds. In spite of the relatively small differences noted among GS-WT liquids, it is noteworthy that the product obtained when Carmeuse was used as a catalyst shows a noticeable faster conversion, followed by GS-WT Dolomite and GS-WT Sand. Relevant differences were also noted when it comes to the microexplosion occurrence size, with GS-WT Dolomite bursting at slightly bigger normalized droplet sizes than GS-WT Carmeuse. The co-pyrolysis liquid obtained without any catalyst (GS-WT Sand) displayed a slower conversion as well as a more delayed microexplosion onset (i.e., the break-up occurred for smaller droplet sizes).

On a final note regarding the evaporation characteristics, it is also worth to mention that all the trends and behaviors extracted from Figure 7 are maintained for all the studied oxygen conditions, keeping the same relative behaviors between fuels irrespective of oxygen availability in the coflow. On the other hand, when comparing a given fuel at different oxygen conditions, it is clear that the enhanced heat transfer due to the apparition of the diffusion flame accelerates the evaporation process, significantly increasing the burning rates.

In addition to the evaporation characteristics, the sooty envelope flames recorded by means of Camera 2 (Figure 2) and displayed in Figure 4 were also post-processed, and their flame size (d_f) was extracted for both combustion conditions. As it is common in the droplet

combustion literature, these results are presented in Figure 8 in terms of the flame standoff ratio (FSR = d_f / d) evolution with normalized residence time.

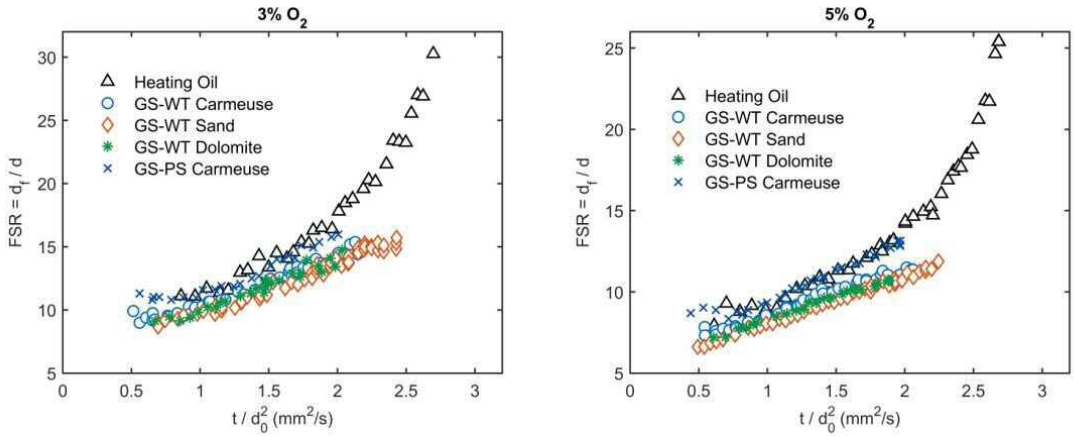

Figure 8. Flame standoff ratio evolution curves for all fuels at both combustion conditions.

The FSR values presented in Figure 8 point to noticeable differences among the studied fuels, with wider flames for heating oil and smaller ones for the GS-WT liquids. This result is consistent with [34], where a tire pyrolysis oil was found to display envelope flames closer to the droplet surface than those of heating oil. GS-PS Carmeuse, on the other hand, shows FSR values intermediate between those of heating oil and GS-WT. For all the studied fuels, the flame standoff ratio shows a sustained growth with the droplet residence time, in disagreement with the classical droplet combustion theory (which predicts a constant FSR value). This feature is caused by the fuel vapour accumulation effect, described in [52] and enhanced for low oxygen availabilities such as those occurring in the current work. A comparison for a given fuel at both oxygen conditions reveals, as expected, an approaching of the flame front to the droplet surface when increasing the O_2 availability in the gaseous coflow, in addition to a lower uncertainty in the experimental data (i.e., lower scattering) due to an improved image quality.

Finally, the soot probe method described in Section 2.4 was applied for all the fuels, obtaining for each of them their corresponding IDSY (Isolated Droplet Soot Yield), defined

in [41] as the soot produced per unit of fuel mass injected under fixed DCF evaporation conditions (150 μm droplets evaporating and pyrolyzing in 0% O_2 coflow). Samples of the particles collected on the filter were analyzed under a scanning electron microscope (SEM), in order to check that the weighed solids corresponded entirely to soot agglomerates and not to other solids which could potentially be formed in the process (e.g., coke particles). A visual analysis of these SEM samples corroborated that virtually all the collected solids are indeed soot agglomerates, without any hint of carbonaceous residues formed through liquid-phase reactions. The soot collection tests were repeated at least three times for each fuel, so that a measure of the experimental uncertainty could be estimated. The average IDSY obtained for each fuel is presented in Figure 9, along with uncertainty bars calculated as twice the measurements' standard deviation (σ).

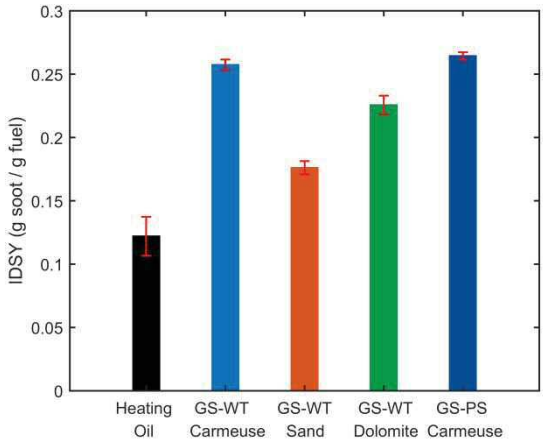

Figure 9. Isolated droplet soot yield (IDSY) obtained for each fuel through the aspirating soot probe tests. The uncertainty bars indicate ± 2 σ of the experimental measurements.

The quantitative results presented in Figure 9 are quite consistent with the qualitative observations in Section 3.2.1. As suggested in Figure 4 by the more luminous shell flames, the longer soot trails and the earlier clustering of these trails into thick agglomerates observed

for GS-PS Carmeuse, Figure 9 confirms that this oil showed the highest propensity to form soot. This result is also consistent with the GC-MS analysis presented in Table 3, where it was shown that this oil displays the largest amount of aromatic compounds (96.9%). On the other hand, GS-WT Carmeuse appears to produce a soot yield quite close to that of GS-PS, even if its aromaticity is noticeably lower (70.9%). It is however worth to note that the distribution of single and multi-ringed aromatics plays a major role in the soot yielded by a fuel, as there are wide differences between the sooting tendency of single-ringed aromatics and that of multi-ringed (e.g., see [53]). Thus, it could be possible that even if GS-WT Carmeuse has a considerably lower total aromatic fraction, it has a higher multi-ring / single-ring ratio. This fuel was also found in Figure 4 to display the second longest soot trails as well as the second earliest clustering of these soot trails into agglomerates. The latter observation seems to concur remarkably well with the soot probe results for all the studied fuels, as it can be observed by comparing Figure 9 and Figure 4. The GS-WT oil produced without any catalyst (GS-WT Sand) yielded the lowest amount of soot among all the co-pyrolysis oils, with GS-WT Dolomite displaying an ISDY value in between those of GS-WT Carmeuse and Sand. All these liquids yielded a significant higher soot weight when compared with heating oil, as it can be corroborated in Figure 9. This is ascribed to the noticeably higher aromatic content of the co-pyrolysis liquids (58.0 - 96.9% according to Table 3 vs. only a 26.2 % in heating oil, as presented in [41]).

4. CONCLUSIONS

In this work, different bio-oils were produced in an auger reactor, aiming to study both the effect of changing the polymer type in the feedstock and the nature of the catalyst for a given biomass-polymer ratio. The physicochemical analysis performed to these organic fractions concluded that the introduction of a catalyst significantly decreased the liquid viscosity and

density, being this effect more marked when using Carmeuse than when employing Dolomite. GS-WT Carmeuse also displayed a noticeable lower oxygen content than GS-WT Dolomite and GS-WT Sand, as well as a lower water fraction. This is thought to be caused by the CaO dehydration capacity, which also enhances the heating value of the liquids obtained with this catalyst. Regarding the chemical composition, the introduction of the Carmeuse catalyst increased the aromatic content compared to Dolomite and Sand, as a result of aromatization and hydrodeoxygenation reactions. From these data, the use of a catalyst (and, more specifically, the Carmeuse type) seems to significantly improve the bio-liquid characteristics. The second variable of study was the polymer type. In this regard, the main difference between GS-WT Carmeuse and GS-PS Carmeuse was the considerably higher aromatic content and the viscosity reduction when using PS as polymer source. This is thought to be caused by the thermal scission of PS, which seemed to heavily reduce phenol and esters content through hydro-deoxygenation route in GS-PS compared to GS-WT.

The second part of this study analyzed the main droplet combustion characteristics of the aforementioned liquids.. The main characteristic of all the bio-oils studied is the occurrence of microexplosions, which achieved in most cases a second atomization of the droplet. This feature is beneficial for liquid conversion in the combustion chamber, as it significantly shortens the droplet lifespan even below that of a conventional heating oil. Among the four studied liquids, the bigger differences were found when changing the polymer source. Namely, GS-PS Carmeuse displayed a considerably more volatile behavior during the initial stage, probably caused by a richer composition in compounds with low boiling point. This fuel also showed the most efficient microexplosions, and therefore its evaporation behavior is considered to be, in global terms, the best among all the explored bio-oils. The GS-WT oils displayed more similar behaviors among them, which are also found to be akin to that of a tire pyrolysis liquid (TPL) studied under the same experimental conditions in a previous

work. Smaller yet noticeable differences were found between the three GS-WT liquids, with a more volatile behavior for GS-WT Carmeuse, a slower conversion for the oil produced without catalyst (GS-WT Sand), and an intermediate behavior for GS-WT Dolomite.

Regarding the propensity to form soot, all the explored bio-liquids displayed a substantially higher soot yield than heating oil, as verified by the aspirating soot probe tests and the imaging observations. These results are consistent with the high aromatic content of the bio-liquids, and could be a drawback when it comes to their combustion in boilers. In this regard, the highest soot yield was measured for both fuels using the Carmeuse catalyst, whereas the liquid obtained without catalyst (GS-WT Sand) produced the lowest soot tendency, probably due to its lower aromaticity and higher oxygen content. In spite of these high sooting levels, a quite positive feature common to all the studied bio-oils is the fact that a SEM analysis of the collected solid particles only revealed soot agglomerates, without any hint of carbonaceous coke-like solids, a common issue when burning certain bio-oils, and which is reported to be detrimental to most combustion applications.

ACKNOWLEDGMENTS

This work was financed by the Spanish Ministry of Economy, Industry and Competitiveness and EU FEDER funds through research projects ENE2016-76436-R and ENE2015-68320-R, by the Spanish Ministry of Education through the pre-doctoral grant FPU15/01866 and the Regional Government of Aragon (DGA) under the research groups call. The authors also would like to thank the help of Luis Ojeda with the droplet combustion experimental tasks.

REFERENCES

[1] A. Ahtikoski, J. Heikkilä, V. Alenius, M. Siren, Economic viability of utilizing biomass energy from young stands—the case of Finland, Biomass and Bioenergy 32 (2008) 988-996.

[2] F. Abnisa, W.M.A.W. Daud, A review on co-pyrolysis of biomass: an optional technique to obtain a high-grade pyrolysis oil, Energy Conversion and Management 87 (2014) 71-85.

[3] A. Imran, E.A. Bramer, K. Seshan, G. Brem, An overview of catalysts in biomass pyrolysis for production of biofuels, Biofuel Research Journal 5 (2018) 872-885.

[4] A. Bridgwater, D. Meier, D. Radlein, An overview of fast pyrolysis of biomass, Organic Geochemistry 30 (1999) 1479-1493.

[5] B. Van de Beld, E. Holle, J. Florijn, The use of pyrolysis oil and pyrolysis oil derived fuels in diesel engines for CHP applications, Applied Energy 102 (2013) 190-197.

[6] A.V. Bridgwater, Review of fast pyrolysis of biomass and product upgrading, Biomass and Bioenergy 38 (2012) 68-94.

[7] Q. Xiong, Y. Yang, F. Xu, Y. Pan, J. Zhang, K. Hong, G. Lorenzini, S. Wang, Overview of computational fluid dynamics simulation of reactor-scale biomass pyrolysis, Chemical Engineering 5(4) (2017) 2783-2798.

[8] K. Dingab, Q. Xiong, Z. Zhong, D. Zhong, Y. Zhang, CFD simulation of combustible solid waste pyrolysis in a fluidized bed reactor, Powder Technology 362 (2020) 177-187.

[9] S. Aramideh, Q. Xiong, S-C. Kong, R.C. Brown, Numerical simulation of biomass fast pyrolysis in an auger reactor, Fuel 156 (2015) 234-24.

[10] A.V. Bridgwater, Renewable fuels and chemicals by thermal processing of biomass, Chemical Engineering Journal 91 (2003) 87-102.

[11] S. Czernik, A. Bridgwater, Overview of applications of biomass fast pyrolysis oil, Energy & Fuels 18 (2004) 590-598.

[12] H.A. Baloch, S. Nizamuddin, M. Siddiqui, S. Riaz, A.S. Jatoi, D.K. Dumbre, N. Mubarak, M. Srinivasan, G. Griffin, Recent advances in production and upgrading of bio-oil from biomass: A critical overview, Journal of Environmental Chemical Engineering 6 (2018) 5101-5118.

[13] O. Sanahuja-Parejo, A. Veses, J.M. López, R. Murillo, M.S. Callén, T. García, Ca-based Catalysts for the Production of High-Quality Bio-Oils from the Catalytic Co-Pyrolysis of Grape Seeds and Waste Tyres, Catalysts 9 (2019) 992.

[14] J. Alvarez, M. Amutio, G. Lopez, L. Santamaria, J. Bilbao, M. Olazar, Improving bio-oil properties through the fast co-pyrolysis of lignocellulosic biomass and waste tyres, Waste Management 85 (2019) 385-395.

[15] B.B. Uzoejinwa, X. He, S. Wang, A.E.-F. Abomohra, Y. Hu, Q. Wang, Co-pyrolysis of biomass and waste plastics as a thermochemical conversion technology for high-grade biofuel production: Recent progress and future directions elsewhere worldwide, Energy Conversion and Management 163 (2018) 468-492.

[16] J.D. Martínez, A. Veses, A.M. Mastral, R. Murillo, M.V. Navarro, N. Puy, A. Artigues, J. Bartrolí, T. García, Co-pyrolysis of biomass with waste tyres: Upgrading of liquid bio-fuel, Fuel Processing Technology 119 (2014) 263-271.

[17] J.D. Martínez, N. Puy, R. Murillo, T. García, M.V. Navarro, A.M. Mastral, Waste tyre pyrolysis–A review, Renewable and Sustainable Energy Reviews 23 (2013) 179-213.

[18] M. Sienkiewicz, H. Janik, K. Borzędowska-Labuda, J. Kucińska-Lipka, Environmentally friendly polymer-rubber composites obtained from waste tyres: A review, Journal of Cleaner Production 147 (2017) 560-571.

[19] L. Zhang, Z. Bao, S. Xia, Q. Lu, K.B. Walters, Catalytic pyrolysis of biomass and polymer wastes, Catalysts 8 (2018) 659.

[20] X. Zhang, H. Lei, S. Chen, J. Wu, Catalytic co-pyrolysis of lignocellulosic biomass with polymers: a critical review, Green Chemistry 18 (2016) 4145-4169.

[21] O. Sanahuja-Parejo, A. Veses, M. Navarro, J. López, R. Murillo, M. Callén, T. García, Catalytic co-pyrolysis of grape seeds and waste tyres for the production of drop-in biofuels, Energy Conversion and Management 171 (2018) 1202-1212.

[22] O. Sanahuja-Parejo, A. Veses, M.V. Navarro, J.M. López, R. Murillo, M.S. Callén, T. García, Drop-in biofuels from the co-pyrolysis of grape seeds and polystyrene, Chemical Engineering Journal 377 (2018) 120246.

[23] A. Veses, O. Sanahuja-Parejo, M. Navarro, J. López, R. Murillo, M. Callén, T. García, From laboratory scale to pilot plant: Evaluation of the catalytic co-pyrolysis of grape seeds and polystyrene wastes with CaO, Catalysis Today, (2020). https://doi.org/10.1016/j.cattod.2020.04.054

[24] K.-L. Pan, J.-W. Li, C.-P. Chen, C.-H. Wang, On droplet combustion of biodiesel fuel mixed with diesel/alkanes in microgravity condition, Combustion and Flame 156 (2009) 1926-1936.

[25] T. Li, D. Zhu, N. Akafuah, K. Saito, C. Law, Synthesis, droplet combustion, and sooting characteristics of biodiesel produced from waste vegetable oils, Proceedings of the Combustion Institute 33 (2011) 2039-2046.

[26] Y.C. Liu, A.J. Savas, C.T. Avedisian, The spherically symmetric droplet burning characteristics of Jet-A and biofuels derived from camelina and tallow, Fuel 108 (2013) 824-832.

[27] Y. Xu, C.T. Avedisian, Combustion of n-butanol, gasoline, and n-butanol/gasoline mixture droplets, Energy & Fuels 29 (2015) 3467-3475.

[28] C.R. Shaddix, D.R. Hardesty, Combustion properties of biomass flash pyrolysis oils: final project report (No. SAND99–8238), Sandia National Labs., Albuquerque, NM (US); Sandia National Labs., Livermore, CA (US), 1999.

[29] C.R. Shaddix, P.J. Tennison. Effects of char content and simple additives on biomass pyrolysis oil droplet combustion, Symposium (International) on Combustion (1998), 1907-1914.

[30] M. Garcia-Perez, P. Lappas, P. Hughes, L. Dell, A. Chaala, D. Kretschmer, C. Roy, Evaporation and combustion characteristics of biomass vacuum pyrolysis oils, IFRF Combustion Journal 200601 (2006) 1-27.

[31] S. Yang, M. Wu, The droplet combustion and thermal characteristics of pinewood bio-oil from slow pyrolysis, Energy 141 (2017) 2377-2386.

[32] G.-B. Chen, Y.-H. Li, C.-H. Lan, H.-T. Lin, Y.-C. Chao, Micro-explosion and burning characteristics of a single droplet of pyrolytic oil from castor seeds, Applied Thermal Engineering 114 (2017) 1053-1063.

[33] S.-S. Hou, F.M. Rizal, T.-H. Lin, T.-Y. Yang, H.-P. Wan, Microexplosion and ignition of droplets of fuel oil/bio-oil (derived from lauan wood) blends, Fuel 113 (2013) 31-42.

[34] Á. Muelas, M.S. Callén, R. Murillo, J. Ballester, Production and droplet combustion characteristics of waste tire pyrolysis oil, Fuel Processing Technology 196 (2019) 106149.

[35] A. Veses, B. Puértolas, M. Callén, T. García, Catalytic upgrading of biomass derived pyrolysis vapors over metal-loaded ZSM-5 zeolites: Effect of different metal cations on the bio-oil final properties, Microporous and Mesoporous Materials 209 (2015) 189-196.

[36] B. Puértolas, A. Veses, M.S. Callén, S. Mitchell, T. García, J. Pérez-Ramírez, Porosity–acidity interplay in hierarchical ZSM-5 zeolites for pyrolysis oil valorization to aromatics, ChemSusChem 8 (2015) 3283-3293.

[37] S. Stefanidis, S. Karakoulia, K. Kalogiannis, E. Iliopoulou, A. Delimitis, H. Yiannoulakis, T. Zampetakis, A. Lappas, K. Triantafyllidis, Natural magnesium oxide (MgO) catalysts: a cost-effective sustainable alternative to acid zeolites for the in situ upgrading of biomass fast pyrolysis oil, Applied Catalysis B: Environmental 196 (2016) 155-173.

[38] A. Veses, M. Aznar, I. Martínez, J.D. Martínez, J.M. López, M.V. Navarro, M.S. Callén, R. Murillo, T. García, Catalytic pyrolysis of wood biomass in an auger reactor using calcium-based catalysts, Bioresource Technology 162 (2014) 250-258.

[39] A. Veses, M. Aznar, M.S. Callén, R. Murillo, T. García, An integrated process for the production of lignocellulosic biomass pyrolysis oils using calcined limestone as a heat carrier with catalytic properties, Fuel 181 (2016) 430-437.

[40] Á. Muelas, P. Remacha, J. Ballester, Droplet combustion and sooting characteristics of UCO biodiesel, heating oil and their mixtures under realistic conditions, Combustion and Flame 203 (2019) 190-203.

[41] A. Muelas, D. Aranda, J. Ballester, Alternative Method for the Formulation of Surrogate Liquid Fuels Based on Evaporative and Sooting Behaviors, Energy & Fuels 33 (2019) 5719-5731.

[42] L.G.G. Pereira, C.A.M. Pires, Bio-oil viscosity of sisal residue: process and temperature influence, Energy & Fuels 32(4) (2018) 5115-5124.

[43] C.C. Elliott, A. Oasmaa, D. Meier, F. Preto, A.V. Bridgwater, Results of the IEA Round Robin on Viscosity and Aging of Fast Pyrolysis Bio-oils: Long-Term Tests and Repeatability, Energy & Fuels 26(12) (2012) 7362-7366.

[44] J.P. Diebold, A review of the chemical and physical mechanisms of the storage stability of fast pyrolysis bio-oils, In Fast Pyrolysis of Biomass: A Handbook Vol. 2, Bridgwater A.V.Ed.; CPL Press, Newbury, 2002; pp. 243-292.

[45] M. Ringer, V. Putsche, J. Scahill, Large-scale pyrolysis oil production: A technology assessment and economic analysis, NREL/TP-510-37779, National Renewable Energy Laboratory, Golden, Colorado, 2006.

[46] J.D. Martínez, M. Lapuerta, R. García-Contreras, R. Murillo, T. García, Fuel properties of tire pyrolysis liquid and its blends with diesel fuel,
Energy and Fuels 27 (2013) 3296 – 3305.

[47] A. Marchese, F. Dryer, V. Nayagam, R. Colantonio. Hydroxyl radical chemiluminescence imaging and the structure of microgravity droplet flames, Symposium (International) on Combustion (1996), 1219-1226.

[48] T. Farouk, Y. Liu, A. Savas, C. Avedisian, F. Dryer, Sub-millimeter sized methyl butanoate droplet combustion: Microgravity experiments and detailed numerical modeling, Proceedings of the Combustion Institute 34 (2013) 1609-1616.

[49] Y.C. Liu, Y. Xu, M.C. Hicks, C.T. Avedisian, Comprehensive study of initial diameter effects and other observations on convection-free droplet combustion in the standard atmosphere for n-heptane, n-octane, and n-decane, Combustion and Flame 171 (2016) 27-41.

[50] M. Mikami, N. Kojima, An experimental and modeling study on stochastic aspects of microexplosion of binary-fuel droplets, Proceedings of the Combustion Institute 29 (2002) 551-559.

[51] J. Ballester, C. Dopazo, Experimental study of the influence of atomization characteristics on the combustion of heavy oil, Combustion Science and Technology 103 (1994) 235-263.

[52] C. Law, S. Chung, N. Srinivasan, Gas-phase quasi-steadiness and fuel vapor accumulation effects in droplet burning, Combustion and Flame 38 (1980) 173-198.

[53] D.D. Das, P.C.S. John, C.S. McEnally, S. Kim, L.D. Pfefferle, Measuring and predicting sooting tendencies of oxygenates, alkanes, alkenes, cycloalkanes, and aromatics on a unified scale, Combustion and Flame 190 (2018) 349-364.